An anthropomorphic deformable phantom of the vaginal wall and cavity

Somerwil, Philip C.; Nout, Remi A.; Mens, Jan Willem M.; Kolkman-Deurloo, Inger Karine K.; Van Beekhuizen, Heleen J.; Dankelman, Jenny; Van De Berg, Nick J.

DOI
10.1088/2057-1976/ac1780

Publication date
2021

Document Version
Final published version

Published in
Biomedical Physics and Engineering Express

Biomedical Physics & Engineering Express

ENDORSED BY IPEM Institute of Physics and Engineering in Medicine

PAPER • OPEN ACCESS

An anthropomorphic deformable phantom of the vaginal wall and cavity

To cite this article: Philip C Somerwil *et al* 2021 *Biomed. Phys. Eng. Express* **7** 055019

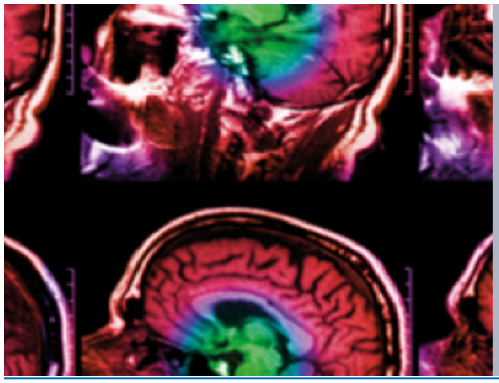

Biomedical Physics & Engineering Express

PAPER

An anthropomorphic deformable phantom of the vaginal wall and cavity

Philip C Somerwil[1], **Remi A Nout**[2], **Jan-Willem M Mens**[2], **Inger-Karine K Kolkman-Deurloo**[2], **Heleen J van Beekhuizen**[3], **Jenny Dankelman**[1] **and Nick J van de Berg**[1,3,*]

[1] Department of Biomechanical Engineering, Delft University of Technology, Delft, The Netherlands
[2] Department of Radiotherapy, Erasmus MC Cancer Institute, University Medical Center Rotterdam, Rotterdam, The Netherlands
[3] Department of Gynaecological Oncology, Erasmus MC Cancer Institute, University Medical Center Rotterdam, Rotterdam, The Netherlands
[*] Author to whom any correspondence should be addressed.

E-mail: n.j.vandeberg@tudelft.nl

Keywords: vaginal wall, vaginal cavity, phantom, anthropomorphic model, biomechanics, PVA, silicone

OPEN ACCESS

RECEIVED
28 May 2021

REVISED
13 July 2021

ACCEPTED FOR PUBLICATION
23 July 2021

PUBLISHED
16 August 2021

Abstract

Brachytherapy is a common treatment in cervical, uterine and vaginal cancer management. The technique is characterised by rapid developments in the fields of medical imaging, dosimetry planning and personalised medical device design. To reduce unnecessary burden on patients, assessments and training of these technologies should preferable be done using high-fidelity physical phantoms. In this study, anthropomorphic deformable phantoms of the vaginal wall and cavity were developed for image-guided adaptive brachytherapy, in which vaginal wall biomechanics were mimicked. Phantoms were produced from both silicone and polyvinyl alcohol materials. Material characterisations were performed with uniaxial tensile tests, via which Young's moduli and toughness were quantified. In addition, the contrast between adjacent phantom layers was quantified in magnetic resonance images. The results showed that stress-strain curves of the silicone phantoms were within the range of those found in healthy human vaginal wall tissues. Sample preconditioning had a large effect on Young's moduli, which ranged between 2.13 and 6.94 MPa in silicone. Toughness was a more robust and accurate metric for biomechanical matching, and ranged between 0.23 and 0.28 $\cdot 10^6$ J$\cdot$m^{-3} as a result of preconditioning. The polyvinyl alcohol phantoms were not stiff or tough enough, with a Young's modulus of 0.16 MPa and toughness of 0.02 $\cdot 10^6$ J$\cdot$m^{-3}. All materials used could be clearly delineated in magnetic resonance images, although the MRI sequence did affect layer contrast. In conclusion, we developed anthropomorphic deformable phantoms that mimic vaginal wall tissue and are well visible in magnetic resonance images. These phantoms will be used to evaluate the properties and to optimise the development and use of personalised brachytherapy applicators.

1. Introduction

1.1. Clinical background

Cervical cancer accounts for an annual 604,127 new cases and 341,831 deaths worldwide. This is equivalent to 7.7% of deaths in women due to cancer [1]. Early stage cervical cancer is typically treated by surgery, including conisation and (radical) hysterectomy. The extent of surgery depends on the tumour stage, defined by the Féderation Internationale de Gynécologie et d'Obstétrique (FIGO) and the Union for International Cancer Control (UICC) TNM systems. In locally advanced and lymph node positive cervical cancer, chemoradiation consisting of external beam radiotherapy combined with weekly cisplatin chemotherapy followed by brachytherapy (BT) is the standard of care. BT plays an important role in the radiotherapy management as it delivers a high and conformal dose to the tumor with maximal sparing of surrounding normal tissue [2]. Brachytherapy is a complex and rapidly developing field, branching to disciplines such as image analysis and radiation physics. Examples of developments include automatic tumour segmentation [3], automated treatment planning [4], *in-vivo* dose monitoring [5], and 3D-printing of patient-specific applicators [6–8].

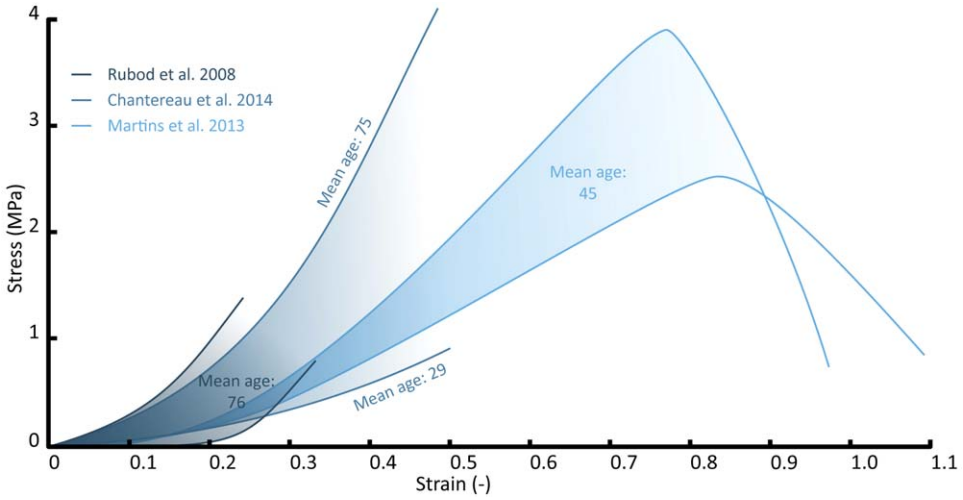

Figure 1. Stress-strain curves of healthy human vaginal wall tissues, as presented in three cadaver studies. Chantereau *et al* compared samples collected from young and old women. For the other two studies, the mean age is indicated.

To minimize patient burden during technological development and evaluation, some steps can and should take place in a preclinical setting. This can be done using either computer-based models, physical patient models or phantoms. For gynaecological BT, a model of the female pelvis is needed that includes the vaginal cavity, vaginal walls, cervix, uterus, and possibly surrounding organs (bladder, rectum, sigmoid) and ligaments. Model complexity may depend on assessment objectives. Although female pelvis phantoms are commercially available, they tend to be expensive, focus on medical imaging training, and present a single idealised anatomical configuration. In addition, they often contain thermoplastic or thermosetting polymers that do not match biomechanical tissue properties. As a result, these phantoms are particularly ill-suited to test personalised health solutions and cases in which inter-patient variability in topology or deformation responses are of importance.

1.2. Related work

The female reproductive system is built to sustain astonishing deformations, especially during pregnancy and labour [9]. Biomechanical tissue properties are complex and hormone-regulated and vary as a result of pregnancy, age, menopause, BMI, and pelvic floor disorders, e.g. pelvic organ prolapse (POP) [10–15]. For the vaginal wall, it has also been shown that smooth muscle content decreases in women with POP [16]. Properties of healthy vaginal wall tissue were examined in a limited number of studies. Typically, stress-strain relations were derived by means of uniaxial tensile testing, results of which are shown in figure 1. These stress-strain relations were often summarized with a Young's modulus. Reported values of healthy vaginal tissue ranged between 6.7–10.5 MPa [13, 17]. However, this linear biomechanical metric is inadequate [12], as the stress-strain relations are hyperelastic.

Related work in phantom design provided physical models of the male pelvis [18–20]. In addition, non-deformable female pelvis models were made for optimisations in radiomics [21]. Nattagh *et al* developed a phantom to train transrectal ultrasound image-guided needle insertion and suturing of the cervix [22]. Kadoya *et al* developed a deformable phantom of the vaginal cavity, uterus, bladder and rectum to assess deformable image registration [23]. Campelo *et al* made a phantom for BT training based on direct 3D phantom printing [24]. Although this is a convenient production method, mimicking biomechanics can be difficult as printable elastomers available today are still limited. The last two articles evaluated Shore hardness values via indentation tests. No articles were found in which large material strains were assessed and used to develop female pelvis phantoms.

Deformable materials used in pelvis models included silicone and polyvinyl alcohol (PVA) [18], agarose gel and silicone [19], carrageenan gel [20], gelatin and rubber [22], urethane and silicone [23] and 3D printable photopolymers [24]. Silicone is a widely used tissue-mimicking material with a high durability [25]. In addition, it has been shown that PVA can be suitable to mimic needle-tissue interactions [26], which may become relevant in BT tasks when interstitial needles are used. We therefore decided to evaluate both silicone and PVA materials.

1.3. Goal

The goal of our study is to develop anthropomorphic and deformable phantoms of the vaginal wall and cavity, with which we can assess and further develop tools and software to assist image-guided adaptive BT. The topology of these phantoms was based on MR images. Uniaxial tensile tests were performed to assess

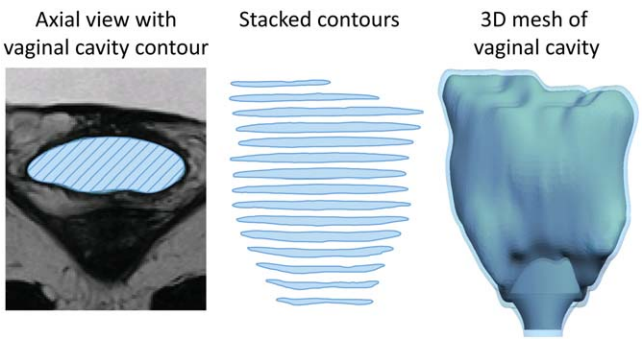

Figure 2. The anthropomorphic vaginal wall model was made using vaginal wall contours drawn in axial MR images. A generic cylindrical base was added to the model. Reproduced From [6]. CC BY 4.0.

the biomechanical response of phantom materials and compare them to vaginal wall tissue properties found in literature. This is the first study in which vaginal wall tissue is matched with phantom materials by looking at large-strain situations, i.e. the stress-strain curves instead of surface indentations. This is crucial when the organ itself may also be subjected to large strains. Stress-strain curves yielded the parameters Young's modulus and toughness (area under the curve). In addition, material layer contrast comparisons were performed in magnetic resonance images (MRI) to quantify relative phantom layer visibility. These phantoms can serve to evaluate personalised applicator fits and ease of insertion or removal, intuitiveness in use during needle placement, and to train vaginal wall contouring and applicator reconstruction in MR images.

2. Methods

2.1. Anthropomorphic design

The vaginal cavity topology was derived from anonymised MRI data, see figure 2. Treatment planning software (Oncentra-Brachy, Elekta, Sweden) was used to segment the vaginal cavity. Contours were saved as DICOM RT-structure files and a surface mesh model was constructed using the SlicerRT extension of 3D Slicer [27]. This model was exported as an STL file and processed further in a computer-aided design program (SolidWorks, Dassault, Systemes, USA). Based on the 3D model of the female pelvic described by Kraima *et al* [28], the outer vaginal wall contour was constructed by non-uniform scaling, using a 2 mm wall thickness. The mould was created using the SolidWorks cavity function. At this stage, surrounding tissue support was simplified by suspending the model in mixtures of PVA and silicone with a lower stiffness.

2.2. Phantom materials

PVA samples were produced by mixing tap water and cooling liquid (C&C automotive Type D/G12, Jodima, Belgium) at a 3:2 weight ratio. PVA powder (99+% hydrolysed PVA, Sigma-Aldrich, USA) was added to create a 12 wt% mixture. The mixture was stirred magnetically (250 rpm) while being heated up to 93 °C and kept at this temperature for 30 min using a control heat plate (IKA C-MAG HS 7, IKA England Ltd, United Kingdom). The mixture was left to cool to 50 °C–65 °C before being injected into the mould with a syringe. The silicone samples (Smooth-Sil™ 940, Smooth-on, USA) consisted of two components that were mixed manually at a 10:1 ratio. A 10 wt% thinner (Silicone Thinner™, Smooth-on, USA) was added to improve filling of the vaginal wall mould. To mimic supportive surrounding tissue, lower stiffness versions of PVA (8 wt%, 2 cycles) and silicone (SORTA-Clear™ 18, Smooth-on, USA) were used.

2.3. Moulds

Three types of moulds were created from polylactic acid (PLA) with a 3D filament printer (Ultimaker 3, Ultimaker, The Netherlands). To determine stress-strain curves, modified dog-bone samples were made, as shown in figure 3(A). Four Silicone 940 samples, ten Silicone 940 + thinner samples, and ten PVA 12% samples were made. The cross-sectional surface area of these samples at the strained region was 30 mm^2 (10 × 3 mm). To evaluate material visibility in MRI, blocks (length, width, height = 50, 50, 40 mm) with cylindrical holes (radius, height = 10, 25 mm) were made, as shown in figure 3(C). Finally, anthropomorphic phantom moulds were created (figure 3(D)). The mould contained four interlocking parts, surrounding a core. In addition, outer support structures were printed for the floor and top of the mould, to keep parts together. The core had the shape of the vaginal cavity and was created using a water-soluble PVA 3D printing filament. The core was centred with four bolts. The mould contained four filling reservoirs at the top, with slanted channels running to the enclosed space. The mould was filled in sequence with silicone and PVA. Air was able to escape via the space between the mould and the central core. Figure 3(E) shows the fully assembled mould with silicone in the reservoirs. After curing of the silicone and PVA phantoms, the structure was suspended in an acrylic

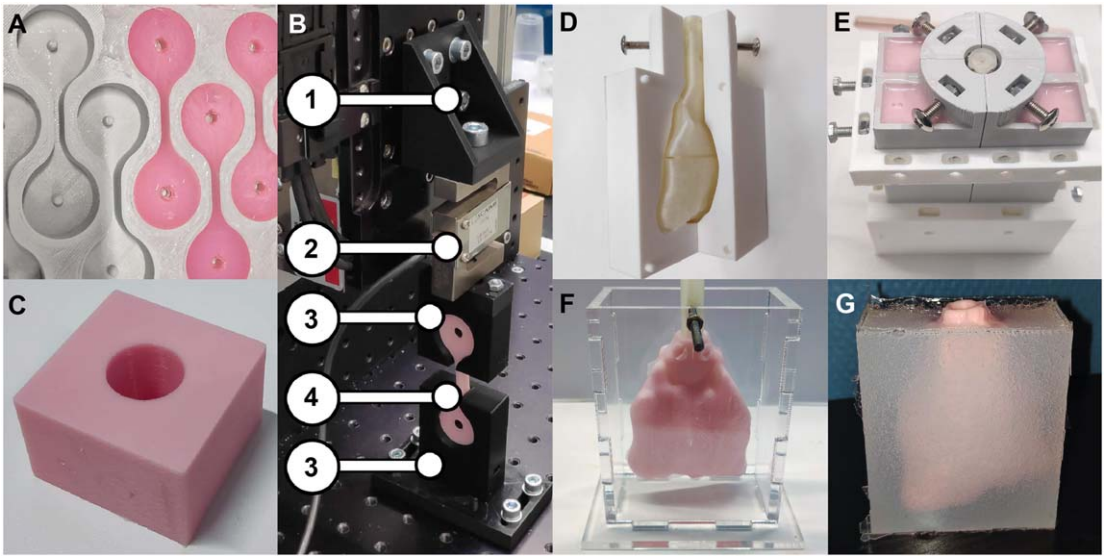

Figure 3. Material testing and designing of phantoms by creating dog-bone shaped test samples of silicone and PVA (A), that were clamped in a uniaxial tensile testing set-up (B), consisting of a mount to a linear stage (1), force sensor (2) and a sample clamp (4) that uses both shape-locking (3) and bolt fixations. Phantom blocks with cylindrical holes were made from the same materials to test visibility in MRI (C). These holes could be filled with ultrasound gel. An anthropomorphic vaginal cavity mould with a soluble core was 3D printed (D), and filled with PVA/silicone (E), to create vaginal wall phantoms, that were subsequently suspended in a container (F) to add a block of surrounding material with a lower stiffness (G).

container (figure 3(F)). The container was filled with the softer supportive material to facilitate phantom handling and positioning. Finally, the insert was dissolved in water and the phantom was ready to use (figure 3(G)).

2.4. Uniaxial tensile testing

A customised linear stage was used for uniaxial tensile testing (figure 3(B)), containing a linear actuator (ACT115DL Direct-Drive, Aerotech, USA) and a linear encoder (RGH22S50F61, Renishaw, United Kingdom) to measure platform location with 0.1 μm precision. A controller (Soloist CP and PWM Digital Drive, Aerotech, USA) was used to control stage movements. For all runs, a constant stage speed of 0.5 mm s^{-1} was used. Tensile force data were acquired using a load cell (ZFA 25 kg, Scaime, France), which was positioned between the upper tissue clamp and the fixture to the stage. The sensor output was amplified (CPJ-CPJ2S analog signal conditioner, Scaime, France) and sent to a computer (USB Multi-function I/O Device NI USB-6008, National Instruments, USA).

2.5. Stress-strain data processing

Data were recorded at a sample rate of 200Hz. Stored data were post-processed in Matlab (R2019b, Mathworks, USA) by means of a moving average filter with a kernel size of 50. Stress was defined as the force normalised per unit of cross-sectional area of the sample, in N m^{-2} or Pa. Strain was defined as the change in length divided by the original length (L), i.e. $\Delta L/L$ or l-L/L (-), where l is the final sample length.

Tissue biomechanics were summarised using the Young's modulus and the area under the mean stress-strain curves. The slope of the stress-strain curve was determined with a linear least squares fit and evaluated along a running window of 1000 data points (5 s). This enabled a search for the largest slope in the 20%–60% strain region, which was considered to be the Young's modulus. The area under the stress-strain curve was determined using a trapezoidal numerical integration of the mean stress-strain curve for strains up to 60%.

2.6. Material visibility in MRI

Dosimetry plans in BT are often constructed with the use of MR images. We therefore evaluated the contrast of adjacent phantom layers using an Optima MR450w 1.5T scanner (GE Healthcare, Chicago, USA). Samples were placed on an MR-compatible tray (figure 4(A)). The second coil was positioned above the tray in accordance with standard pre-BT MRI treatment protocols. Standard MRI sequences used in gynaecological BT were used for imaging, of which the T2-weighted fast recovery fast spin echo scan (FRFSE) with TR/TEeff = 2986ms/103ms and T1-weighted 2-point Dixon radio-frequency spoiled gradient echo scan (LAVA Flex) using TR/TE/flip angle = 6.7ms/4.5ms/10° were selected to compare phantom layers, see figures 4(B) and 4(C).

In addition to the phantoms, standardised blocks of silicone and PVA were produced, see figure 3(C) and figure 4(A). These blocks contained a cylindrical cavity to quantify contrast with ultrasound gel (supragel, LCH medical products, France), which is used in clinical practice to distend the vaginal cavity and enhance contrast to facilitate contouring [29]. Image

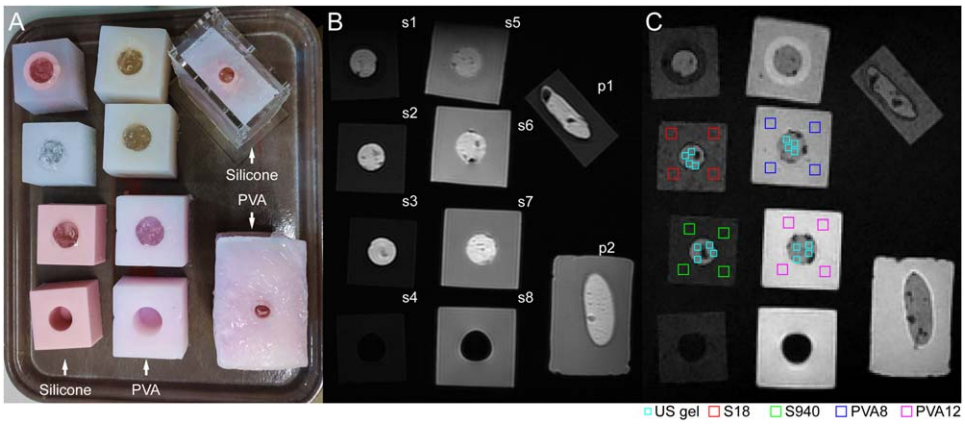

Figure 4. Photo of the collection of silicone and PVA materials on an MR-compatible tray (A). An MR image (FRFSE) was obtained (B) of the samples, containing the materials: s1 (S18, S940, US gel), s2 (S18, US gel), s3 (S940, US gel), s4 (S940, air), s5 (PVA8, PVA12, US gel), s6 (, PVA8, US gel), s7 (PVA12, US gel), s8 (PVA12, air). The phantoms contained the material layers: p1 (S18, S940, US gel), p2 (PVA8, PVA12, US gel). A second MR image (LAVA Flex) was obtained (C) of the same samples. Here, the regions of interest are shown in four specimens, which were used for relative material contrast quantifications.

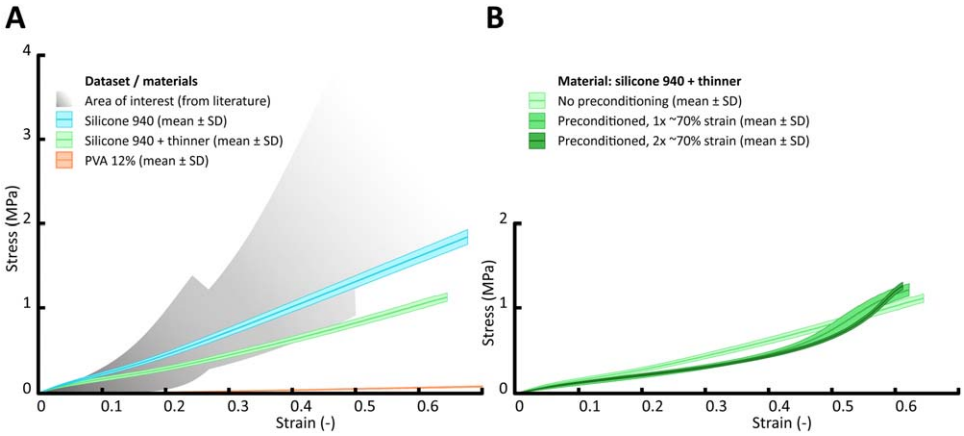

Figure 5. Stress-strain curves obtained by uniaxial tensile tests of Silicone 940, Silicone 940+ thinner, and PVA 12% dog-bone samples (A). The effect of material preconditioning is shown by applying 1–3 times a ~70% strain on the samples (B).

data were stored in DICOM format and contrast was analysed in Matlab. For each sample layer, the average of four regions of interest was determined, as shown in figure 4(C). Air pockets and shadows, which were mostly seen in the ultrasound gel filling, were avoided.

Contrast was determined in normalised FRFSE and LAVA Flex images, in which pixel intensity ranged between [0,1]. Contrast was defined as $|\tilde{I}_{FG}-\tilde{I}_{BG}|$, where $\tilde{I}_{FG}$ is the mean pixel intensity of the foreground layer and $\tilde{I}_{BG}$ the mean pixel intensity of the background layer. To summarize material visibility, contrast values were averaged for samples that compared the same adjacent materials.

3. Results

3.1. Stress-strain curves

The results of the uniaxial tensile tests are shown in figure 5(A). In addition, the area of interest of stress-strain curves of vaginal wall tissue of healthy patients is shown, as derived from literature (see Introduction). The curves are furthermore summarised by means of the Young's modulus (YM) and area under the curve (AUC) in table 1. From the curves, it can be seen that the silicone samples resemble the vaginal wall biomechanics, in particular when low to moderate elongations (<50%) are applied. The PVA samples have a much lower stiffness. Figure 5(B) shows the effect of preconditioning for Silicone 940 with a thinner. It appears that preconditioning increases the non-linearity of the stress-strain curve. This is visible from the Young's modulus, which increases rapidly (table 1).

3.2. Visibility in MRI

Data on the relative contrast of structures in multi-layered phantoms in MR images are presented in table 2. In addition, the contrast of these materials relative to ultrasound gel is shown. The multi-layered silicone and PVA structures could best be distinguished with the LAVA Flex sequence (contrast in

Table 1. Biomechanical phantom material properties[a].

	S940	S940T	S940T 1× pc	940T 2× pc	PVA12
YM	2.99	2.13	4.66	6.94	0.16
AUC	0.46	0.28	0.24	0.23	0.02

[a] YM: Young's modulus (MPa) and AUC: area under the curve (10^6 J·m^{-3}), derived from the mean stress-strain curves of Silicone 940 (S940), Silicone 940+ thinner (S940T), and PVA 12% (PVA12). The effect of preconditioning (1× pc, 2× pc, at 70% strain) is also shown for material S940T.

Table 2. Contrast in FRFSE (left bottom, bold) and LAVA Flex (right top) sequences, quantified as mean intensity differences of adjacent layers[a].

	US gel	S18	S940	PVA8	PVA12
US gel		0.16	0.27	0.15	0.29
S18	**0.46**		0.11	—	—
S940	**0.48**	**0.01**		—	—
PVA8	**0.21**	—	—		0.12
PVA12	**0.29**	—	—	**0.04**	

[a] Contrast values were obtained by sampling four foreground (FG) and four background (BG) regions of interest per imaged sample. Relative material contrast was obtained by averaging values of samples with the same material combinations.

silicone: 0.11, and in PVA: 0.12). The contrast was much lower in the FRFSE sequence (silicone: 0.01 and PVA: 0.04).

4. Discussion

Deformable anthropomorphic phantoms of the vaginal wall and cavity were produced with PVA and silicone materials. The topology of these phantoms was based on MR images, and tissue biomechanics were studied and compared to vaginal wall properties found in literature. Surrounding tissues were represented by a low-stiffness alternative of PVA and silicone, respectively. The obtained stress-strain curves of the silicone phantoms are within the range of those found in vaginal wall tissues. In comparison, the PVA phantoms lack in stiffness and toughness. As the description of hyperelastic materials with a linear fit and Young's modulus is inaccurate, we have also quantified material toughness using the area under the stress-strain curve. This area describes strain energy per unit of volume. However, comparative clinical values are still missing. In addition, the contrast of material combinations was evaluated in MRI. In particular with the LAVA Flex MRI sequence all materials selected could be distinguished.

The phantoms produced can serve many purposes. Phantoms can be of value for training, e.g., to counter recently found limits in confidence of residents in developing a BT practice [30]. During training, variation in cases is very important to avoid repetitive non-comprehensive learning [24]. The presented patient-driven approach can provide these variations. In addition, the phantom may be used to assess applicator introduction to- and removal from the vaginal cavity, and mechanical solutions to facilitate this, e.g., by splitting applicators in dove-tailing pieces that can be inserted in sequence [8]. They can be made alongside personalised applicators to test user-friendliness and to train vaginal wall contouring and applicator reconstruction in MR images.

A limitation of the materials used is that they could not mimic the strong hyperelasticity of vaginal wall tissue, which result from the anisotropic fibrous networks. The vaginal wall consists mostly of smooth muscle, collagen and elastin and is arranged in four layers: the epithelium, the subepithelium, the muscularis, and the adventitia [9]. The subepithelium provides passive mechanical support via randomly aligned fibres, whereas the muscularis provides active mechanical support via smooth muscle cells that are oriented in the longitudinal direction of the vagina. The adventitia provides connections to surrounding organs, such as the bladder and rectum. Although it is known that the force response differs between longitudinal and transverse samples [31], and between samples of the anterior and posterior wall [32], tissue anisotropy still needs to be studied in more detail. In the end these hyperelastic responses may be mimicked in multi-layered or fibre-reinforced phantoms. For a high-fidelity mechanical response, mimicking connections to adjacent structures, i.e., mechanical boundary conditions, will be equally important.

Next steps in our phantom design include the introduction of the uterus, as well as zones to treat (tumours) and avoid (organs at risk). This enables imaging and dosimetric planning in MRI to assess dose conformity obtained after implementing intracavitary and interstitial needles with conventional and personalised applicators. Here, the ability of phantom materials to mimic needle-tissue interactions may become important. For each intended use, it is important to balance model fidelity and complexity. For many assessment and training purposes, model simplifications may be justifiable.

In conclusion, we have developed anthropomorphic deformable phantoms that mimic vaginal wall tissue and are well visible in magnetic resonance imaging. In terms of the biomechanical response, the developed silicone phantoms provided a close correspondence to mechanical behaviour of the vaginal wall. These phantoms will be used to evaluate the properties and to optimise development and utilisation of personalised brachytherapy applicators.

Acknowledgments

This work was supported by the Dutch Research Council (NWO), grant nr. 17921.

Data availability statement

The data generated and/or analysed during the current study are not publicly available for legal/ethical reasons but are available from the corresponding author on reasonable request.

ORCID iDs

Nick J van de Berg https://orcid.org/0000-0001-6291-990X

References

[1] Sung H *et al* 2021 Global cancer statistics 2020: GLOBOCAN estimates of incidence and mortality worldwide for 36 cancers in 185 countries *Ca-Cancer J Clin* **71** 209–49
[2] Cibula D *et al* 2018 The european society of gynaecological oncology/european society for radiotherapy and oncology/european society of pathology guidelines for the management of patients with cervical cancer *Virchows Arch.* **472** 919–36
[3] Torheim T *et al* 2017 Autodelineation of cervical cancers using multiparametric magnetic resonance imaging and machine learning *Acta Oncol.* **56** 806–12
[4] Oud M *et al* 2020 Fast and fully-automated multi-criterial treatment planning for adaptive HDR brachytherapy for locally advanced cervical cancer *Radiother. Oncol.* **148** 143–50
[5] Carrara M *et al* 2017 Clinical application of Moskin dosimeters to rectal wall *in vivo* dosimetry in gynecological HDR brachytherapy *Phys Medica.* **41** 5–12
[6] Laan R C, Nout R A, Dankelman J and van de Berg N J 2019 MRI-driven design of customised 3D printed gynaecological brachytherapy applicators with curved needle channels *3D Print Med.* **5** 8
[7] Magne N, Chargari C, SanFilippo N, Messai T, Gerbaulet A and Haie-Meder C 2010 Technical aspects and perspectives of the vaginal mold applicator for brachytherapy of gynecologic malignancies *Brachytherapy.* **9** 274–7
[8] Wiebe E, Easton H, Thomas G, Barbera L, D'Alimonte L and Ravi A 2015 Customized vaginal vault brachytherapy with computed tomography imaging-derived applicator prototyping *Brachytherapy.* **14** 380–4
[9] Baah-Dwomoh A, McGuire J, Tan T, De and Vita R 2016 Mechanical properties of female reproductive organs and supporting connective tissues: a review of the current state of knowledge *Appl. Mech. Rev* **68** 060801
[10] Goh J T W 2002 Biomechanical properties of prolapsed vaginal tissue in pre- and postmenopausal women *Int Urogynecol J Pel.* **13** 76–9
[11] Rahn D D, Ruff M D, Brown S A, Tibbals H F and Word R A 2008 Biomechanical properties of the vaginal wall: effect of pregnancy, elastic fiber deficiency, and pelvic organ prolapse *Am J Obstet Gynecol* **198** 590
[12] Rubod C, Boukerrou M, Brieu M, Jean-Charles C, Dubois P and Cosson M 2008 Biomechanical properties of vaginal tissue: preliminary results *Int Urogynecol J* **19** 811–6
[13] Martins P *et al* 2013 Biomechanical properties of vaginal tissue in women with pelvic organ prolapse *Gynecol Obstet Inves* **75** 85–92
[14] Chantereau P, Brieu M, Kammal M, Farthmann J, Gabriel B and Cosson M 2014 Mechanical properties of pelvic soft tissue of young women and impact of aging *Int Urogynecol J.* **25** 1547–53
[15] Lopez S O, Eberhart R C, Zimmern P E and Chuong C J 2015 Influence of body mass index on the biomechanical properties of the human prolapsed anterior vaginal wall *Int Urogynecol J.* **26** 519–25
[16] Badiou W, Granier G, Bousquet P J, Monrozies X, Mares P and de Tayrac R 2008 Comparative histological analysis of anterior vaginal wall in women with pelvic organ prolapse or control subjects. A pilot study *Int Urogynecol J.* **19** 723–9
[17] Lei L L, Song Y F and Chen R Q 2007 Biomechanical properties of prolapsed vaginal tissue in pre- and postmenopausal women *Int Urogynecol J.* **18** 603–7
[18] Cunningham J M, Barberi E A, Miller J, Kim J P and Glide-Hurst C K 2019 Development and evaluation of a novel MR-compatible pelvic end-to-end phantom *J Appl Clin Med Phys.* **20** 265–75
[19] Niebuhr N I *et al* 2019 The ADAM-pelvis phantom-an anthropomorphic, deformable and multimodal phantom for MRgRT *Phys. Med. Biol.* **64** 04NT05
[20] Singhrao K *et al* 2020 A novel anthropomorphic multimodality phantom for MRI-based radiotherapy quality assurance testing *Med. Phys.* **47** 1443–51
[21] Bianchini L *et al* 2020 PETER PHAN: an mri phantom for the optimisation of radiomic studies of the female pelvis *Phys Medica.* **71** 71–81
[22] Nattagh K, Siauw T, Pouliot J, Hsu I C and Cunha J A 2014 A training phantom for ultrasound-guided needle insertion and suturing *Brachytherapy.* **13** 413–9
[23] Kadoya N *et al* 2017 Evaluation of deformable image registration between external beam radiotherapy and HDR brachytherapy for cervical cancer with a 3D-printed deformable pelvis phantom *Med. Phys.* **44** 1445–55
[24] Campelo S, Subashi E, Meltsner S G, Chang Z, Chino J and Craciunescu O 2020 Multimaterial three-dimensional printing in brachytherapy: prototyping teaching tools for interstitial and intracavitary procedures in cervical cancers *Brachytherapy.* **19** 767–76
[25] Ehrbar S *et al* 2019 ELPHA: dynamically deformable liver phantom for real-time motion-adaptive radiotherapy treatments *Med. Phys.* **46** 839–50
[26] de Jong T L, Pluymen L H, van Gerwen D J, Kleinrensink G J, Dankelman J and van den Dobbelsteen J J 2017 PVA matches human liver in needle-tissue interaction *J Mech Behav Biomed.* **69** 223–8
[27] Fedorov A *et al* 2012 3D Slicer as an image computing platform for the Quantitative Imaging Network *Magn. Reson. Imaging* **30** 1323–41
[28] Kraima A C *et al* 2013 Toward a highly-detailed 3D pelvic model: approaching an ultra-specific level for surgical simulation and anatomical education *Clin. Anat.* **26** 333–8
[29] Ferreira D M *et al* 2015 Magnetic resonance imaging of the vagina: an overview for radiologists with emphasis on clinical decision making *Radiol Bras.* **48** 249–59
[30] Marcrom S R *et al* 2019 Brachytherapy training survey of radiation oncology residents *Int J Radiat Oncol.* **103** 557–60
[31] Peña E *et al* 2011 Mechanical characterization of the softening behavior of human vaginal tissue *J Mech Behav Biomed.* **4** 275–83
[32] Jean-Charles C, Rubod C, Brieu M, Boukerrou M, Fasel J and Cosson M 2010 Biomechanical properties of prolapsed or non-prolapsed vaginal tissue: impact on genital prolapse surgery *Int Urogynecol J.* **21** 1535–8